scientific reports

Check for updates

OPEN

Degradation kinetics of Andrographolide in aqueous solution, product identification and biological activity evaluation

Wuttichai Jaidee[1], Narawadee Rujanapun[1], Kulawadee Malee[1], Suchada Chaisawadi[2], Panupong Puttarak[3,4], Poonsit Hiransai[5,6], Geoffrey A. Cordell[7,8], Satyajit D. Sarker[9], Lutfun Nahar[10] & Rawiwan Charoensup[1,11]✉

Andrographolide (1) is a labdane-type diterpene lactone and the major bioactive metabolite (2.39%) in the leaves of *Andrographis paniculata* (Acanthaceae). To further explore its stability, the thermal degradation kinetics of compound 1 at pH 2.0, pH 6.0, and pH 8.0 were modeled at three temperatures within 50–85 °C. The activation energy (E_a), shelf-life ($t_{90\%}$), and rate constant (*k*) for compound 1 were determined using the Arrhenius equation. Consequently, the results indicated that degradation followed first-order kinetics, and the optimum pH for stability was determined to be between pH 2.0 and 4.0. Major degradation products formed under pH 2.0 and pH 6.0 conditions were isolated and spectroscopically characterized by comparison with known compounds. Under pH 2.0 conditions, two degradation products were identified: isoandrographolide (2) and 8,9-didehydroandrographolide (3). Under pH 6.0 conditions, three degradation products were formed: 15-*seco*-andrographolide (4), 14-deoxy-15-methoxyandrographolide (5), and 11,14-dehydro-14-deoxyandrographolide (6). Anti-inflammatory and cytotoxicity assessments demonstrated reduced biological effects for the degradation products compared with compound 1. This highlights the importance of controlling pH during formulation to ensure product stability, sustained bioactivity, and patient benefit.

Keywords Andrographolide, Degradation, pH dependency, Product characterization, Arrhenius equation, NO production, Cytotoxicity

Andrographis paniculata (Burm. f.) Wall. (Acanthaceae) is listed in Thailand's National Drug List (2016) and is known for its medicinal uses, particularly in treating digestive and respiratory conditions. It is recommended for relieving the symptoms of the common cold and non-infectious diarrhea[1]. The leaves of *A. paniculata* were listed as the Herbal Champion and Products Champion in 2023, as one of the top medicinal plants identified for potential export from Thailand[2]. This plant is commonly used in traditional medicine systems throughout Southeast Asia[3].

Andrographolide (**1**), a labdane diterpenoid, is the major biochemical marker responsible for the pharmacological effects of *A. paniculata*[3] and the highest level of **1** is found in the leaves (2.39%) about 130 days after initial cultivation[4]. It has various biological effects, including anticancer, antioxidant, antimicrobial, anti-

[1]Medicinal Plant Innovation Center of Mae Fah Luang University, Mae Fah Luang University, Chiang Rai 57100, Thailand. [2]Pilot Plant Development and Training Institute, King Mongkut's University of Technology Thonburi, Bangkok 10150, Thailand. [3]Phytomedicine and Pharmaceutical Biotechnology Excellence Center, Faculty of Pharmaceutical Sciences, Prince of Songkhla University, Hat-Yai, Songkhla 90110, Thailand. [4]Department of Pharmacognosy and Pharmaceutical Botany, Faculty of Pharmaceutical Sciences, Prince of Songkhla University, Hat-Yai, Songkhla 90110, Thailand. [5]Center of Excellence in Marijuana, Hemp, and Kratom, Walailak University, Nakhon Si Thammarat 80160, Thailand. [6]School of Allied Health Sciences, Walailak University, Nakhon Si Thammarat 80160, Thailand. [7]Natural Products Inc., Evanston, IL 60201, USA. [8]College of Pharmacy, University of Florida, Gainesville, FL 32610, USA. [9]Centre for Natural Products Discovery, School of Pharmacy and Biomolecular Sciences, Liverpool John Moores University, Byrom Street, Liverpool L3 3AF, UK. [10]Laboratory of Growth Regulators, Palacký University and Institute of Experimental Botany, The Czech Academy of Sciences, Šlechtitelů 27, 78371 Olomouc, Czech Republic. [11]School of Integrative Medicine, Mae Fah Luang University, Chiang Rai 57100, Thailand. ✉email: rawiwan.cha@mfu.ac.th

inflammatory, antiviral, antidiabetic, and wound-healing properties[5–10]. Recent research has shown that **1** has potent activity against the SARS-CoV-2 virus, with an IC_{50} value of 0.034 μM[10–12]. Furthermore, it is utilized as a chemical marker for the quality control of various dosage forms, including solid, liquid, and semi-solid formulations[13]. The stability and biological activity of medicinal agents can affect their performance following formulation studies to enhance the bioavailability. Thus, to accommodate alternative formulation approaches and longer storage times, to retain the biological effects and to define a product life-time, stability must be assured. This is essential information for the design of different formulations, to reduce the variability in the systemic and topical drug levels over time, and to ensure product consistency and effectiveness for the patient. Like many highly functionalized biological agents, the stability of **1** is influenced by the processing and storage conditions and by the pH during manufacture and delivery which may impact the efficacy of a final product[13,14]. However, the stability behavior of **1** is not yet fully understood, and the biological activities of the degradation products requires further examination.

Considering the present and possible future clinical applications of andrographolide (**1**) several different types of formulation might be prepared relevant to the product use[13]. Consequently, an intimate knowledge of the thermal and acid-base stability of **1** is necessary to predict the possible degradation processes resulting from exposure to varied temperatures and pH during unit operations, and the consequent outcomes on bioefficacy. These production processes include, and are not limited to, the handling and storage of the raw plant material, the method of extraction and concentration, the conditions for formulation into products (such as baking, extrusion processing, pasteurization, or sterilization), and the time and temperature factors during storage of the product, prior to and during clinical application[15]. Current knowledge regarding the thermal stability and kinetics of purified **1** and the biological responses of its degradation products is limited. Some studies have reported on stability of **1** under specific storage conditions and during heat-accelerated stress-testing, following ICH Q1A(R2) guidelines for the stability testing of new drug substances and products. For instance, Garg et al.[16] found that **1** remains stable under mild acidic conditions, in oxidative environments, with dry heat, and after photochemical degradation. There was no significant reduction in the content of **1** in *A. paniculata* when stored at 5 °C under ambient conditions over three months[17]. However, studies of the stability of **1** in *A. paniculata* powder over extended time periods are notably scarce, with only a single report by Ahammed et al.[18]. The stability of the ground leaf material and solid **1** under heat-accelerated conditions revealed decomposition through a second-order kinetics process, with the primary degradation product identified as **6**[19,20]. Earlier research demonstrated the heat-accelerated and long-term storage degradation of **1** in the solid-state[16–18,21,22].

First-order reaction kinetics for the degradation of **1** were observed in aqueous solutions[23] and the degradation products under acidic and basic conditions were identified as **3**, **4**, and **6**[24]. Under varying pH conditions, **1** is readily transformed[16,17,19–25] although there is limited knowledge regarding these structural changes through isolation and structure elucidation and their impact on the diverse biological responses induced by **1**.

The aims of this study were to assess the effects of temperature and solution pH on the degradation kinetic rates and the products of **1**. Thermal degradation kinetic modeling was used to establish the kinetic parameters (the order of reaction and reaction rate constant) and to predict the shelf-life ($t_{90\%}$). In addition, the effects of these structural changes of **1** on the in vitro anti-inflammatory activity and cytotoxicity of the degradation products were assessed.

Materials and methods

General experimental procedures

The NMR spectra were recorded using a Bruker, Avance NEO, 500 MHz Nuclear Magnetic Resonance Spectrometer (NMR). NMR grade MeOH-d_4, was purchased from Cambridge Isotope Laboratories, Inc. (Tewksbury, MA, USA) for use as a NMR solvent. HPLC grade acetonitrile (ACN), methanol (MeOH), analytical grade dimethyl sulfoxide (DMSO), and potassium dihydrogen phosphate (KH_2PO_4) were purchased from RCI Labscan (Bangkok, Thailand). Sodium hydroxide pellets (NaOH) were acquired from QReC™ (Auckland, New Zealand). Potassium chloride (KCl) was from Kemaus Chemicals (Cherrybrook, New South Wales, Australia). Sodium bicarbonate ($NaHCO_3$) was obtained from Ajax Finechem (Taren Point, New South Wales, Australia). HPLC-grade water was prepared using Elix essential 5 UV + Milli-Q reference A, ultra-purification water systems (Merck Millipore, Darmstadt, Germany) in series. The samples were filtered through a PTFE, 13 mm, 0.2 μm membrane (Agilent, Santa Clara, USA) prior to chromatography. The andrographolide (**1**) standard (500 mg) was purchased from Sigma-Aldrich (St. Louis, MO, USA, purity 98%, Product # 365645, Lot # MKCP5983). LC-MS/MS studies were conducted at Mae Fah Luang University, Thailand using an Agilent LC-QTOF 6500 system (Santa Clara, CA, USA). The MS method parameters and the UPLC conditions for the dissolution apparatus are listed in the Supplementary Table S1.

Chemical kinetics in selected pH solutions

The effect of pH on the chemical stability of **1** in solution was studied at temperatures in the range 50–85 °C (Table S2). Solutions were prepared at selected pH conditions between pH 2.0–pH 12.0, namely, pH 2.0 (0.2 M HCl + 0.2 M KCl), pH 4.0 (0.1 M KH_2PO_4 + 0.2 M HCl), pH 6.0 (0.1 M KH_2PO_4 + 0.1 M NaOH), pH 8.0 (0.1 M KH_2PO_4 + 0.1 M NaOH), pH 10.0 (0.05 M $NaHCO_3$ + 0.1 M NaOH), and pH 12.0 (0.05 M $NaHCO_3$ + 0.1 M NaOH)[13]. The pHs were measured using a Mettler Toledo Sevencompact pH/Ion S220 instrument (Greifensee, Switzerland).

The pH 2.0, 6.0, and 8.0 solutions were incubated separately at 70, 77, and 85 °C, and samples (100 μL) at 0–35 days for pH 2.0, 0–11 days for pH 6.0, and 0–3.5 h for pH 8.0 were transferred to a vial containing methanol (900 μL) to produce a stock solution of 200 μg/mL (Table 1). The solutions were analyzed directly after the solution was prepared. The experiments were performed in triplicate.

pH of solution								
pH 2.0			pH 6.0			pH 8.0		
Temp. (°C)	k_d (per day)	(r^2)	Temp. (°C)	k_d (per day)	(r^2)	Temp. (°C)	k_d (per day)	(r^2)
70	0.0323	0.9800	60	0.0804	0.9714	50	1.2172	0.9514
77	0.0966	0.9804	70	0.2314	0.9975	60	2.7249	0.9978
85	0.1866	0.9928	80	0.4360	0.9933	70	6.8275	0.9926

Table 1. Degradation rate constants of **1** in pH 2.0, pH 6.0, and pH 8.0 solutions at selected temperatures, estimated using a first-order kinetics model. k_d : equilibrium dissociation constant r^2: the coefficient of determination

Kinetics of the degradation of 1

The reaction order kinetics of the chemical degradation of **1** were established by plotting concentration (C), ln(C), or 1/C against time[15]. The correlation coefficients (r^2 were calculated for these plots and demonstrated a strong correlation ($0.9514 < r^2 < 0.9978$). The dependence of the rate constant (k) and the activation energy (E_a) on temperature was evaluated using the Arrhenius equation (Eq. 1).

$$\ln k = -\left(\frac{Ea}{R}\right).\frac{1}{T} + \ln\ \mathrm{A} \tag{1}$$

Where: k is a specific reaction rate, A is the pre-exponential factor (per day), E_a is the activation energy (J/mol), T is the absolute temperature (Kelvin), and R is the ideal gas constant (8.31 J/mol K). The plot of the logarithm of the rate constant as a function of $1/T$ results in a straight line with the negative of the slope equal to E_a/R.

The Arrhenius factor indicating the accelerated breakdown of each compound at various temperatures was calculated using the following equation (Eq. 2).

$$A = \mathrm{e}^{\mathrm{x}}. \tag{2}$$

Where x is the y-intercept of the semi logarithmic curve of the Arrhenius plot.

The shelf-life ($t_{90\%}$) for first-order kinetics was calculated from equation (Eq. 3).

$$t_{90\%} = \frac{-\ln(0.9)}{kp} \quad (\text{First - order}) \tag{3}$$

Where k_p is the rate of reaction at the predicted temperature from the Arrhenius plot curve.

Quantitative analysis of 1

The quantitative analysis of **1** from the kinetics experiments was conducted using high-performance liquid chromatography (HPLC) employing an Agilent instrument (Santa Clara, CA, USA) equipped with a 1260 Quat Pump VL and a 1260 DAD detector. Chromatographic separations were carried out on a reverse-phase column: Poroshell EC-C18 column (4.6 × 150 mm, 2.6 µm) (Agilent), maintained at 25 °C. The UV detector was set at 224 nm. The mobile phase for the HPLC analysis consisted of a 1:1 (*v/v*) mixture of water and methanol, based on preliminary experiments which minimized interference from other matrix components. A flow rate of 1 mL/min was maintained throughout the analysis. Prior to HPLC injection, samples were filtered through a PTFE, 13 mm, 0.2 µm membrane filter. To establish a standard calibration curve, a known quantity of **1** standard (10 mg) was dissolved in DMSO (10 mL) to achieve 1.0 mg/mL. Serial dilutions of this stock solution with methanol were performed to create a series of working standards ranging from 3.9 to 500 µg/mL. The standard curve was constructed by plotting the peak areas obtained from the HPLC analysis against the corresponding concentrations.

Isolation of degradation products by HPLC

The analysis and isolation of the degradation products of **1** were accomplished using the HPLC conditions described previously. The degradation products were formed through controlled conditions during the incubation of **1** in acidic (pH 2.0) and basic (pH 8.0) solutions. Samples were treated with a methanol-buffer mixture (2:3) at 70 °C for 22 days for pH 2.0 and for 1 h for pH 8.0. The reactions were monitored periodically, and HPLC analysis was conducted to assess the development of each degradation product. The isolation process enabled the separation of five degradation products of **1** from the reaction mixtures derived from the two pH conditions.

Anti-inflammatory activities of 1 and its degradation products

The anti-inflammatory effects of **1** and its degradation products were assessed using the inhibition of nitric oxide (NO) formation assay at 15–300 µM[25]. The assay exploits the increased NO levels from an induced

inflammatory response in activated macrophages, and the level of inhibition from an exogenous material. RAW264.7 macrophage cells, purchased from ATCC (TIB-71) (Manassas, VA, USA) were cultured and treated with lipopolysaccharide (LPS) to induce an inflammatory response, followed by treatment with the samples for 24 h. The cells were then exposed to varying concentrations of **1** and its degradation products. Nitric oxide (NO) levels were measured using the Griess reagent. To perform the assay, a sample (50 µL) of the culture supernatant was transferred to a new plate and mixed with Griess reagent (50 µL). The reagent reacts with nitrite (the stable product of NO) to produce a colored solution that can be quantified spectrophotometrically at 540 nm[25]. Dose-response curves were generated to determine the IC_{50} for each compound, providing insights into their relative anti-inflammatory efficacy compared to the parent compound **1**. Indomethacin was used as the positive control.

The cytotoxic activity of 1 and its degradation products

The cytotoxic activities of **1** and the degradation products **2**–**6** were evaluated against SW480 human colon cancer cells, purchased from ATCC (Manassas, VA, USA) using the MTT assay[26] at 0.15–150 µM. Doxorubicin was used as the positive control. SW480 cells were selected based on their relevance as a model for studying colon cancer.

Results and discussion

The thermal stability of **1** was assessed kinetically in aqueous solutions at different pH levels relevant to the formulation of commercial products. Andrographolide (**1**) is the major bioactive metabolite of *A. paniculata* and is thus a driver for the development of value-added products, either as a single material or as an ingredient in a standardized mixture. The use of standardized preparations of *A. paniculata* leaves or leaf extracts as functional ingredients for medicinal plant products is also important for commercial development. Knowledge regarding the thermal stability of **1** is therefore of significance for the development of high-quality functional products for the cosmetic and nutraceutical industries. Such standardized extracts and cosmetic products may be exposed to elevated temperatures at different pH levels, depending on the production processes, and may experience a variety of formulation, storage, and manufacturing operations where metabolite integrity could be compromised[13,27,28].

Identification of degradation products

The HPLC method for the analysis of **1** was adapted from the American Herbal Pharmacopoeia[29]. The separation of **1** and its major degradation products from the pH-adjusted solutions in methanol (MeOH) was accomplished within a 25 min time frame. The isolates were characterized using nuclear magnetic resonance (NMR) spectroscopy and mass spectrometry and comparison with published spectroscopic data (Supplementary Tables S3 and S4, Figures S1–S10). In the acidic environment (pH 2.0), the degradation products **2**[30–35] and **3**[24,36] eluted at retention times (t_R) of 4.1 min and 7.6 min, respectively (Fig. 1). Isoandrographolide (**2**), a white amorphous powder, possessed a molecular formula of $C_{20}H_{30}O_5$ as determined by (+)-LC-MS-QTOF $[M+Na]^+$ at *m/z* 373.1976 (Supplementary Figure S11). The ^{1}H- and ^{13}C-NMR spectra of **2** were similar to those of **1**, except for a methyl group at C-17 (δ_H 1.19) and an oxymethine proton at C-12 (δ_H 4.58), instead of an *exo*-methylene group H-7α (δ_H 4.67) and H-7β (δ_H 4.89) and an olefinic proton H-12 (δ_H 6.85) in **1**, respectively (Supplementary Table S3). The ^{13}C NMR data of **2** showed two oxymethine carbons at C-8 (δ_C 83.2) and C-12 (δ_C 72.3) instead of the two resonances of olefinic carbons in **1** (Supplementary Table S4). The NMR data of **2** agree with those reported[35]. 8,9-Didehydroandrographolide (**3**), white amorphous powder, $C_{20}H_{30}O_5$, showing (–)-LC-MS-QTOF at *m/z* 395.2069 $([M+HCOO]^-$ (Supplementary Figure S12). The ^{1}H- and ^{13}C-NMR data were closely related to those of **1**, except for an *endo*-olefinic group at C-8 (δ_C 129.2), C-9 (δ_C 134.9), and C-17 (δ_C 20.9) in **3**, instead of an *exo*-methylene group in **1** (Supplementary Table S4). The NMR spectral data of **3** agreed with those previously reported[24].

For the pH 8.0 solution, the degradation products **4**[3,24,37,38], **5**[39], and **6**[19,20,24] eluted at t_R of 5.5, 10.2, and 19.8 min, respectively. Compound **6** was not detected in strongly basic conditions (pH 10.0–12.0) (Fig. 1). 15-*Seco*-andrographolide (**4**) was isolated as a white amorphous powder, $C_{20}H_{32}O_6$, *m/z* 367.2123 $([M-H]^-)$ (Supplementary Figure S13). The structure of **4** was confirmed by comparison of the NMR data with **1**, through the presence of an acyclic oxy-methylene group at C-15 (δ_H 3.75 and δ_H 3.61; δ_C 66.3) instead of the cyclic oxy-methylene protons (δ_H 4.16 and δ_H 4.46; δ_C 76.1) in **1** (Supplementary Table S3). The NMR data of **4** agreed with those reported[24]. 14-Deoxy-15-methoxyandrographolide (**5**) was obtained as a white solid, $C_{21}H_{32}O_5$, *m/z* 365.2328 $([M+H]^+)$ (Supplementary Figure S14). The NMR data were similar to those of **1**, except for resonances for a methylene at C-14 (δ_H 3.09, 2.67; δ_C 33.5) and di-oxymethine at C-15 (δ_H 5.55; δ_C 104.4), instead of resonances for an oxymethine and oxymethylene in **1**. The structure of **5** was confirmed by comparison of the NMR data with those reported[39]. The structure of 11,14-dehydro-14-deoxy-andrographolide (**6**) was confirmed by analysis of the ^{1}H-NMR data with those reported[24]. A *trans*-olefinic group was observed at C-11 (δ_H 6.86; δ_C 136.54) and C-12 (δ_H 6.16; δ_C 122.5). and by the resonances for an olefinic group at C-13 (δ_C 129.6) and C-14 (δ_H 7.44; δ_C 146.7) instead of an oxy methine in **1**. The (+)-LC-MS-QTOF at *m/z* 333.2060 $([M+H]^+)$ confirmed the molecular formula to be $C_{20}H_{28}O_5$ (Supplementary Figure S15).

The HPLC chromatograms illustrating the degradation products formed at pH 2.0, pH 6.0, and pH 8.0 are presented in Fig. 1 and Supplementary Figures S16–S18. In experiments using DMSO, the degradation product observed under acidic conditions (pH 2.0) produced similar signals as in MeOH, whereas under strongly basic conditions (pH 10.0 and pH 12.0), only **4** was formed from **1** (Supplementary Figure S19). Polarity or nucleophilicity therefore plays an important role in the degradation pathways of **1** since MeOH is a stronger nucleophile than DMSO and thus **5** could be observed in the MeOH conditions.

The persistence of the degradation products from **1** in pH 2.0 solution was evident with compounds detected for at least 7 days (Supplementary Figure S16), whereas at pH 6.0 and pH 8.0 **4** was the major degradation

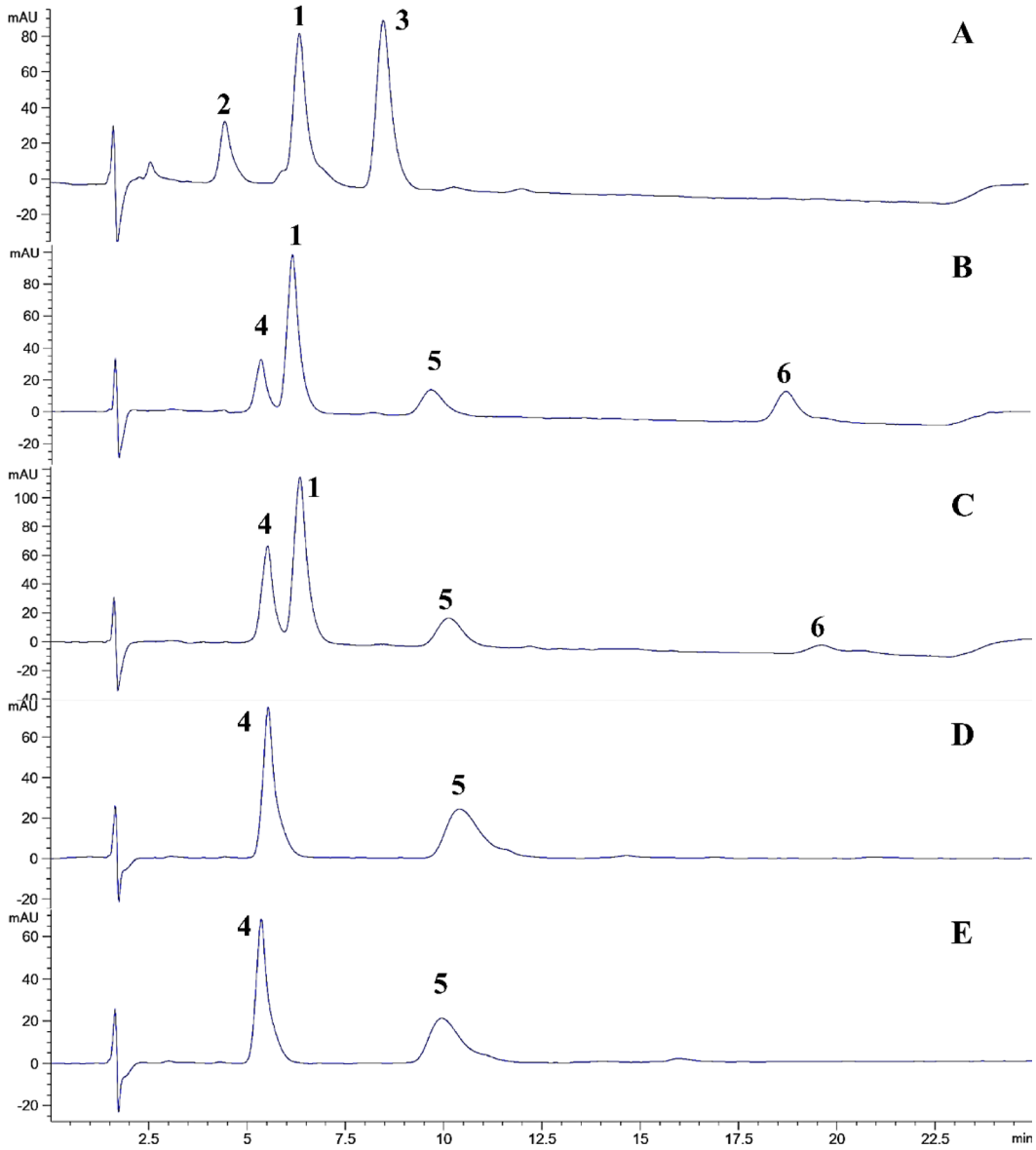

Fig. 1. HPLC chromatograms of pH 2.0, pH 6.0, and pH 8.0 stressed solutions at 70 °C on a Poroshell EC C18 column, flow rate: 1 mL/min, 25 min, 50% MeOH–H_2O, detected at UV 224 nm. **A**; pH 2.0 shows the peaks of **2** (4.1 min), **1** (5.7 min), and **3** (7.6 min). **B** and **C**; pH 6.0 and pH 8.0 showing the peaks for **4** (5.5 min), **1** (5.7 min), **5** (10.2 min), and **6** (19.8 min). **D** and **E**; pH 10.0 and pH 12.0 at 70 °C showing the peaks for **4** (5.5 min) and **5** (10.2 min).

product, and **5** and **6** were observed in small amounts under these conditions (Fig. 1 and Supplementary Figures S17 and S18). The formation of products **4**, **5**, and **6** was initially detected after 2 days at pH 6.0, and after 1 h at pH 8.0 (Supplementary Figures S17 and S18). These studies support the previous reports on the kinetic degradation of **1** in solution[24]. Andrographolide (**1**) therefore undergoes distinctive acid and base-catalyzed degradation pathways which provides a critical insight into the degradation mechanisms of **1** and highlights the importance of pH on the stability and transformation of this bioactive compound when different pharmaceutical or cosmeceutical formulations are being considered.

Kinetics of the degradation of 1

HPLC chromatographic analysis revealed a direct relationship between the pH of the solution and the rate of the degradation reaction. Specifically, at pH 2.0 and pH 4.0, the degradation of **1** occurred at a slower rate compared to solutions at higher pH levels (pH 6.0 to pH 12.0) (Figs. 2 and 3). The HPLC chromatogram of **1** at pH 2.0 over a period of 7 days at 70 °C indicated two degradation products, **2** and **3** (Supplementary Figure S16), while no degradation was detected at pH 4.0 in the same time frame and temperature (Supplementary Figure S20). Thus, **1** exhibited greater stability in pH 4.0 buffer solution compared to pH 2.0, consistent with previous findings that noted the optimal stability of **1** within the pH range of 3–5[40]. Although the degradation rates increase below pH

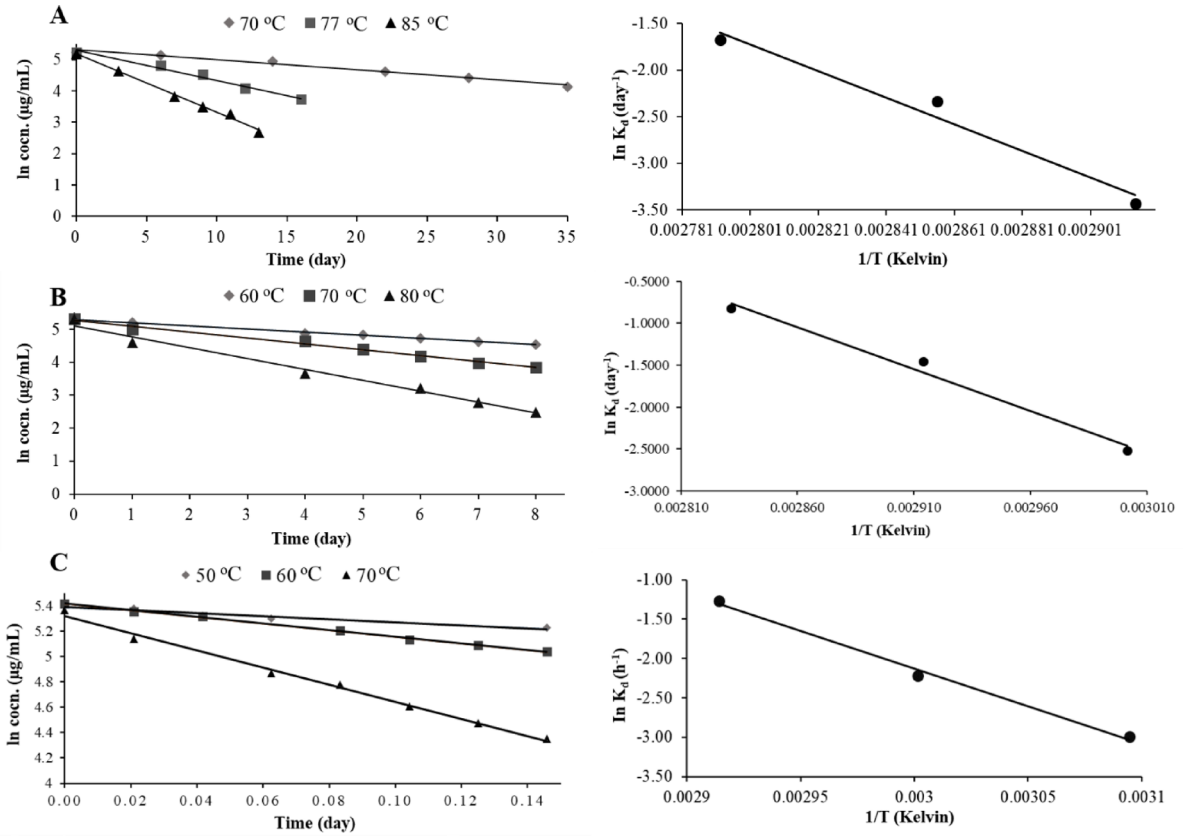

Fig. 2. First-order plot and Arrhenius plots of the degradation of andrographolide based on pH, (**A**) pH 2.0, (**B**) pH 6.0, and (**C**) pH 8.0.

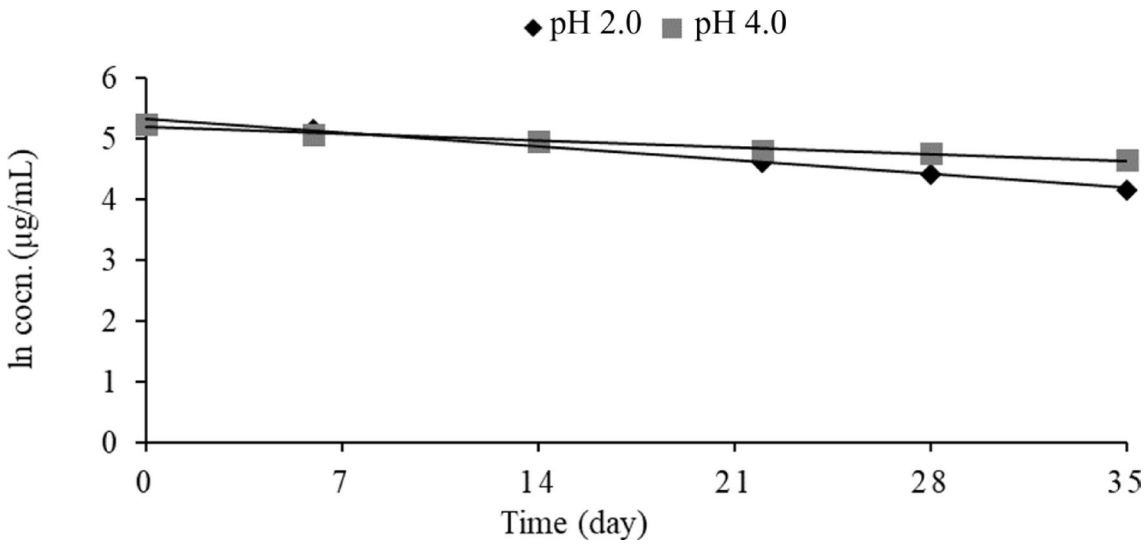

Fig. 3. First-order plot of the degradation of andrographolide (**1**) in MeOH between pH 2.0 and pH 4.0 at 70 °C for 35 days.

3.0, **1** remains largely present at pH 2.0, a typical human gastric value, and making this low pH relevant in the context of food, cosmetic, and drug processing.

The metabolite remained stable at the boiling point of MeOH (64.7 °C for 28 days), whereas in DMSO, the degradation rate of **1** depended on the temperature and the composition of the solvent[23]. The rate constant for the degradation of **1** was investigated at pH 2.0, pH 6.0, and pH 8.0, and at three individualized, elevated temperatures of 70, 77, and 85 °C (Table 1). Chemical kinetic parameters and profiles for the degradation of **1**

are shown in Table 2. As expected, in each case the apparent kinetic rate constant (k) increased with increasing temperature. Strong correlation coefficients ($0.9800 < r^2 < 0.9978$) from the plot of ln (C) against reaction time (day) were found (Table 1). The rate constant obtained from Eq. (1) was fitted to an Arrhenius-type equation in each kinetic model studied to determine the effect of temperature on the chemical reaction (Fig. 2). The k values indicated the decreased thermal stability of **1** as the temperature was increased. Under different conditions, the k value of solid-state andrographolide under heat-accelerating conditions was reported to be 3.8×10^{-6} per day[17] and 6.58×10^{-6} per day[18] while in pH-dependent solutions the k value was revealed as 6.5×10^{-5} per day (at pH 2.0), 2.5×10^{-3} per day (at pH 6.0), and 9.9×10^{-2} per day (at pH 8.0). Thus **1** decomposed faster in acid and basic solutions than in the solid state. This is the first report documenting the thermal degradation kinetics of **1** at specific pH conditions. These results align with earlier studies that characterized the degradation of **1** as following a first-order reaction model in solution through intermolecular interactions[23]. First-order kinetics indicated that the degradation of **1** is concentration dependent, therefore the amount of **1** degrading per unit of time is not constant for the ambient pH conditions. Most drugs tend to degrade with either zero- or first-order kinetics[41]. On the other hand, solid state **1** decomposed through second-order degradation kinetics under accelerated conditions through intramolecular interactions[19,20]. Second-order degradation occurs when the rate is influenced by the concentration of two separate or identical reactants. Therefore, the varied matrix or formulation of **1** under study may be the cause of the identified differences in degradation kinetics. The intermolecular interactions of **1** influence the rate of degradation[17–20]. However, the intramolecular interactions of **1**, particularly through hydrogen bonds and hydrophobic interactions are crucial for stability and function. The calculated activation energies (E_a) derived from the curves showed that the values for **1** at pH 2.0, pH 6.0, and pH 8.0 were 118.9, 82.8, and 79.4 kJ/mol[1], respectively (Table 2). A high E_a generally indicates that the reaction is less sensitive to temperature fluctuations[15]. Hence, the higher E_a value of **1** at pH 2.0 portends a lower sensitivity to temperature-induced degradation than in pH 6.0 and pH 8.0 solutions. The stability of **1** in acidic conditions may be due to the presence of free –OH groups causing clustering, followed by strong intermolecular hydrogen bonding. The shelf-life values for **1** at pH 2.0, pH 6.0, and pH 8.0 at 25 °C were 4.3 years, 41 days, and 1.1 days, respectively (Table 2) which is highly significant for product formulation studies.

Formation of degradation products

The transformation of **1** into **2** can occur through (a) allylic rearrangement of the hydroxyl group on the lactone ring, (b) protonation of the *exo*-methylene group, and (c) cyclization of the tetrahydrofuran ring[30]. The formation of **3** was visualized to occur through isomerization of the 8,17-double bond by (a) protonation of the *exo*-methylene moiety, and (b) abstraction of the proton at C-9[22] (Scheme 1). However, the ^{13}C-NMR spectrum indicated a mixture of formation olefinic isomers of **3** for which the precise configuration could not be established. Compound **4** could be produced through fragmentation of the lactone ring of **1**, and **6** could arise through E2 elimination by base following abstraction of the δ-proton in **1** leading to 1,4-elimination from an allylic alcohol[24] (Scheme 1). The formation of **5** may occur through methoxylation at C-15 involving an enol lactone intermediate (m/z 333.2060)[42] which may be derived from **6** (Scheme 1 and Supplementary Figure S21). However, the ^{1}H-NMR spectrum indicated either a mixture of C-15-epimers of **5**, or only one epimer for which the precise configuration could not be established. This mechanistic possibility was revealed from the HPLC analysis of **5** when **6** was treated at pH 8.0 in MeOH solution (Supplementary Figure S22). This chemical reaction supports the biogenetic pathway for **5** that is proposed to occur in plants[39]. However, **5** could also be an artifact due to the presence of MeOH in the solution which acts as a nucleophile to react with an enol lactone intermediate (Figure 4 and Scheme 1). This analysis enumerates some of the mechanisms underlying the degradation of **1** and highlights the potential for exploring reaction opportunities towards further analogues for biological assessment while retaining their stability.

Biological activity assessments

To investigate the changes in the biological profile of the degradation products in comparison with **1**, two bioassays were performed. The first assay evaluated the inhibitory effect on lipopolysaccharide (LPS)-induced nitric oxide (NO) production in RAW264.7 macrophages. The results of this anti-inflammatory bioassay for **1** and its degradation products are summarized in Table 3. The presence of a newly formed tetrahydrofuran ring and an olefinic bond in **2** did not enhance the anti-inflammatory activity when compared to **1** and the other degradation products. This affirmed that the conjugated $\Delta^{12(13)}$-double bond and the hydroxy group at C-14 are critical structural elements for the inhibition of NO production[33]. In addition, the anti-inflammatory activity of **5** and **6** was not enhanced relative to **1**, **3**, and **4** through the introduction of a methoxy group at C-15 in **5**, and a conjugated double bond in compound **6**. These results align with molecular docking studies on the nitric oxide

Parameter	pH of solution[a]		
	pH 2.0	pH 6.0	pH 8.0
Activation energy (E_a)	118.9 kJ/mol	82.8 kJ/mol	79.4 kJ/mol
Arrhenius frequency factor (A)	4.5×10^{16} per day	8.4×10^{11} per day	8.1×10^{12} per day
Rate constant (k_p) at 25 °C *	6.5×10^{-5} per day	2.5×10^{-3} per day	0.099 per day
Predicted shelf-life ($t_{90\%}$) at 25 °C	4.3 years	41 days	1.1 days

Table 2. Predicted shelf-life ($t_{90\%}$) of **1** in pH 2.0, pH 6.0, and pH 8.0 solutions at 25 °C using an arrhenius method. [a]First-order degradation.

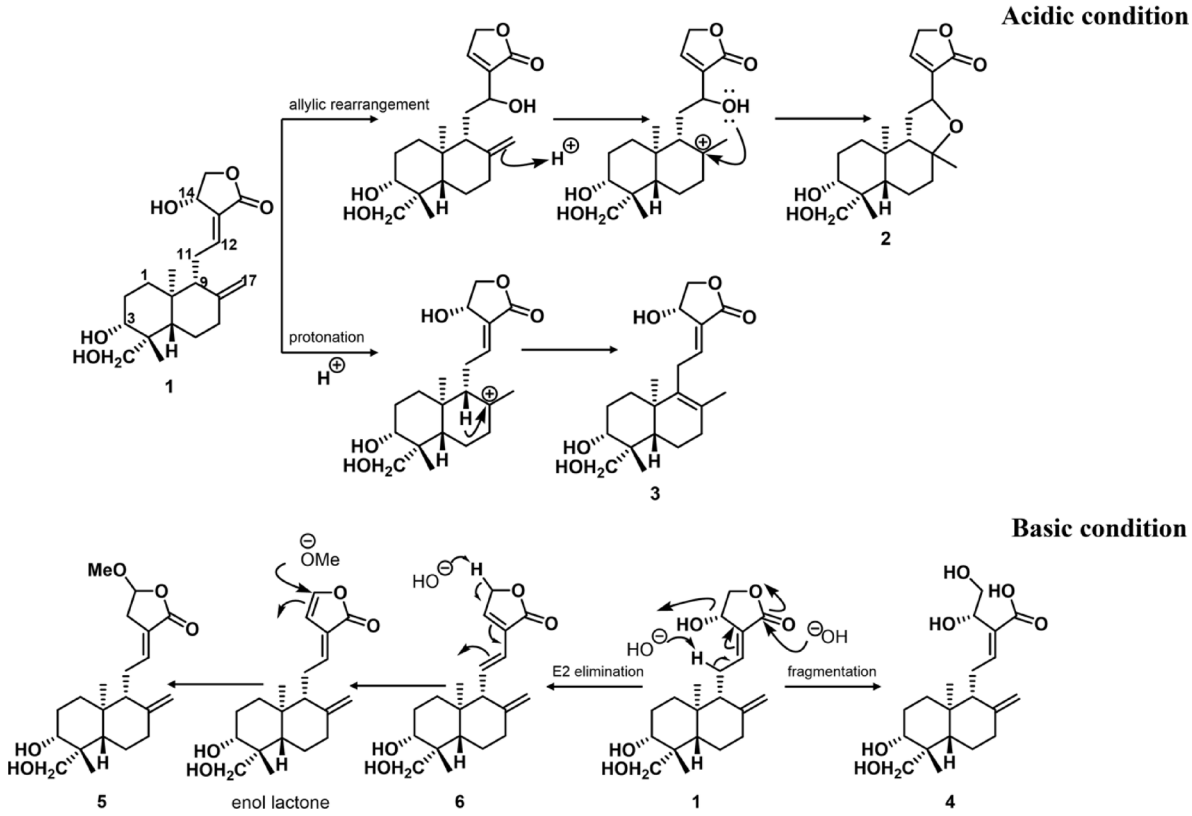

Scheme 1. Reaction mechanisms for the degradation of **1** under acidic and basic conditions.

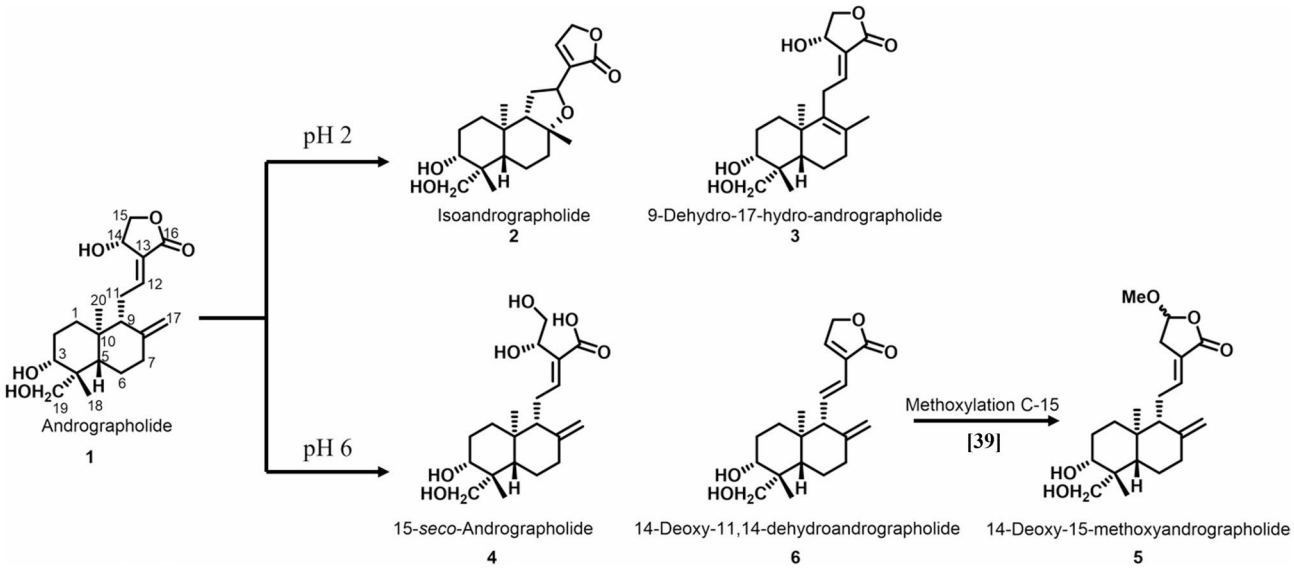

Fig. 4. Chemical structures of **1** and its degradation products.

production inhibition activity of **1** and its derivatives[43]. The formation of a C-8 vinylic methyl group, as in **3**, and **4** where the lactone ring is opened, were less active than **1**. These data confirm that, since in the degradation products of **1** the strong anti-inflammatory activity is not retained, the stability of **1** in formulated medicinal products must be monitored over time to avoid diminished efficacy for the patient. In this study it was affirmed that **1** was extensively degraded under strongly basic conditions. Therefore, alkaline products of **1**, such as soaps and shampoos, can be explored for other activities, recognizing that the anti-inflammatory activity of **1** will have been lost.

Compound	NO production (IC_{50}, μM)	SW480[a] (IC_{50}, μM)		
		24 h	48 h	72 h
1	48.59 ± 0.71	5.08 ± 0.04	4.48 ± 0.52	4.17 ± 0.07
2	250.30 ± 0.90	> 50	> 50	> 50
3	98.41 ± 0.81	26.42 ± 0.67	23.85 ± 0.86	6.25 ± 0.95
4	102.75 ± 0.83	27.08 ± 1.95	20.46 ± 1.99	6.00 ± 0.37
5	123.30 ± 1.98	44.39 ± 5.12	37.12 ± 3.82	16.16 ± 1.26
6	176.87 ± 1.39	> 50	> 50	> 50
Indomethacin [b]	26.47 ± 1.07			
Doxorubicin [b]		0.79 ± 0.06	0.09 ± 0.01	0.09 ± 0.01

Table 3. NO production and cytotoxic activity of **1** and its degradation products **2**–**6**. [a] Human colon cancer cell line [b] Positive control

The cytotoxic activities of the degradation products and **1** were assessed against the SW480 human colon cancer cell line, with the resulting IC_{50} values presented in Table 3. Compounds **2** and **6** exhibited no activity at the tested concentrations, in agreement with earlier studies across a selection of cancer cell lines[42–47]. In this investigation, the parent compound **1** was identified as the most cytotoxic with a modest IC_{50} value of 4.17 μM, suggesting the important role of the allylic hydroxyl lactone moiety of **1** in imparting cytotoxic effects. Compounds with a C-8 vinylic methyl group, e.g., **3**, and with the lactone ring-opened, e.g., **4**, demonstrated weaker cytotoxic activity compared to **1**. In summary, the structural integrity of **1** is necessary for maintaining both the anti-inflammatory and cytotoxic activities in developed products.

Conclusions

The thermal degradation kinetics of the **1** in buffer solutions at pH values ranging from pH 2.0 to pH 8.0 with temperatures ranging from 60 to 85 °C were calculated and successfully applied to predict the shelf-life ($t_{90\%}$). The optimum pH for **1** stability was between pH 2.0 and pH 4.0. The degradation of **1** followed first-order reaction kinetics and the transformation depended on the temperature and the pH, reacting more quickly with increasing temperature and more basic pH values. Five major degradation products, compounds **2**–**6**, were isolated and identified by MS and NMR analyses. Andrographolide (**1**) consistently exhibited the highest potency in terms of anti-inflammatory and cytotoxic activities when compared to its degradation products. To maintain the biological effectiveness of **1**, when incorporated into products, the conditions should incorporate a lower temperature, avoid a strong basic condition, and short-time processing.

Data availability

The datasets used and/or analyzed during the current study available from the corresponding author on reasonable request.

Received: 9 March 2025; Accepted: 25 July 2025
Published online: 07 August 2025

References

1. National Drug Committee, National Essential Drug List Committee, Ministry of Public Health. Bangkok. (2016). https://www.chromeextension.com//efaidnbmnnnibpcajpcglclefindmkaj/https://ndi.fda.moph.go.th/uploads/file_news/202209301360287102.pdf
2. Bangkok Post. List of top herbs eyed for export. (2023). https://www.bangkokpost.com/thailand/general/2479664/list-of-top-herbs-eyed-for-export. Accessed on July 9, 2025.
3. Zhan, S. et al. Synthesis and evaluation of Andrographolide derivatives as potent anti-osteoporosis agents in vitro and in vivo. *Eur. J. Med. Chem.* **21**, 3113185 (2021).
4. Pholphana, N., Rangkadilok, N., Saehun, J., Ritruechai, S. & Satayavivad, J. Changes in the contents of four active diterpenoids at different growth stages in *Andrographis paniculata* (Burm.f.) Nees (Chuanxinlian). *Chin. Med.* **8** (1), 2–12 (2013).
5. Dai, G. F., Xu, H. W., Wang, J. F., Liu, F. W. & Liu, H.-M. Studies on the novel α-glucosidase inhibitory activity and structure-activity relations for Andrographolide analogues. *Bioorg. Med. Chem. Lett.* **16** (10), 2710–2713 (2006).
6. Chen, D., Song, Y., Lu, Y. & Xue, X. Synthesis and in vitro cytotoxicity of andrographolide-19-oic acid analogues as anti-cancer agents. *Bioorg. Med. Chem. Lett.* **23** (11), 3166–3169 (2013).
7. Geng, J., Liu, J., Yuan, X., Liu, W. & Guo, W. Andrographolide triggers autophagy-mediated inflammation Inhibition and attenuates chronic unpredictable mild stress (CUMS)-induced depressive-like behavior in mice. *Toxicol. Appl. Pharmacol.* **379**, 114688 (2019).
8. Paemanee, A., Hitakarun, A., Wintachai, P., Roytrakul, S. & Smith, D. R. A proteomic analysis of the anti-dengue virus activity of Andrographolide. *Biomed. Pharmacother.* **109**, 322–332 (2019).
9. Luo, S. et al. Andrographolide ameliorates oxidative stress, inflammation and histological outcome in complete freund's adjuvant-induced arthritis. *Chem. Biol. Interact.* **319**, 108984 (2020).
10. Adiguna, S. P. et al. Antiviral activities of Andrographolide and its derivatives: Mechanism of action and delivery system. *Pharmaceuticals* **14** (11), 1102–1116 (2021).
11. Intharuksa, A., Arunotayanun, W., Yooin, W. & Sirisa-Ard, P. A. Comprehensive review of *Andrographis paniculata* (Burm. f.) Nees and its constituents as potential lead compounds for COVID-19 drug discovery. *Molecules* **27** (14), 4479–4513 (2022).
12. Banerjee, S. et al. Immunoprotective potential of ayurvedic herb Kalmegh (*Andrographis paniculata*) against respiratory viral infections – LC–MS/MS and network Pharmacology analysis. *Phytochem Anal.* **32**, 629–639 (2021).

13. Raman, S., Murugaiyah, V. & Parumasivam, T. *Andrographis paniculata* dosage forms and advances in nanoparticulate delivery systems: An overview. *Molecules* **27** (19), 6164–6181 (2022).
14. Maiti, K. et al. Enhancing bioavailability and hepatoprotective activity of Andrographolide from *Andrographis paniculata*, a well-known medicinal food, through its herbosome. *J. Sci. Food Agric.* **90**, 43–51 (2010).
15. Jaidee, W. et al. Kinetics of CBD, Δ^9-THC degradation and cannabinol formation in cannabis resin at various temperature and pH conditions. *Cannabis Cannabinoid Res.* **7** (4), 537–547 (2021).
16. Garg, C., Sharma, P., Satija, S. & Garg, M. Stability indicating studies of *Andrographis paniculata* extract by validate HPTLC protocol. *J. Pharmacogn Phytochem*. **5** (6), 337–344 (2016).
17. Ibrahim, M. N. & Chong, G. H. Stability of Andrographolide in *Andrographis paniculata* under selected storage conditions. *Int. J. Eng. Technol.* **5**, 69–73 (2008).
18. Ahammed, M. T., Sultan, M. Z., Hossain, M. S., Mahtab, M. A. & Bachar, S. C. Degradation of Andrographolide in *Andrographis paniculata* over 1 year storage. *Phytochem Anal.* **36** (1), 289–295 (2025).
19. Lomlim, L., Jirayupong, N. & Plubrukarn, A. Heat-accelerated degradation of solid-state Andrographolide. *Chem. Pharm. Bull.* **51** (1), 24–26 (2003).
20. Plubrukarn, A., Pinsuwan, S., Ingkatawornwong, S. & Supavita, T. Stability of Andrographolide in powdered andrographis herb under accelerated conditions. *Planta Med.* **72** (10), 954–956 (2006).
21. Wadeng, A. Degradation profile of chemical constituents in Andrographis herb. Preprint at: (2017). https://kb.psu.ac.th/psukb/handle/2016/11664
22. Jana, S. et al. Quantification and standardization of Andrographolide in *Andrographis paniculata* samples by validated RP-HPLC and HPTLC methods. *J. Chromatogr. Sci.* **61** (6), 514–521 (2023).
23. Wongkittipong, R., Prat, L., Damronglerd, S. & Gourdon, C. Solid–liquid extraction of Andrographolide from plants–experimental study, kinetic reaction and model. *Sep. Purif. Technol.* **40** (2), 147–154 (2004).
24. Phattanawasin, P., Sotanaphun, U., Burana-Osot, J. & Piyapolrungroj, N. Isolation and characterization of the acid and base degradation products of Andrographolide. *Pharmazie* **73** (10), 559–562 (2018).
25. Raksat, A. et al. Antibacterial and inhibitory activities against nitric oxide production of coumarinochromones and prenylated isoflavones from *Millettia extensa*. *J. Nat. Prod.* **82** (8), 2343–2348 (2019).
26. Jaidee, W. et al. Metabolite fingerprinting of *Piper nigrum* L. from different regions of Thailand by UHPLC-QTOF-MS approach and *in vitro* bioactivities. *Trends Sci.* **19** (22), 1520–1532 (2022).
27. Fitrasuah, S. I. et al. Analysis of chemical properties and antioxidant activity of Sambiloto (*Andrographis paniculata* Nees.) leaf tea formula as a functional drink in preventing coronavirus diseases and degenerative diseases. *J. Med. Sci.* **9**, 196–201 (2021).
28. Adeleye, O. A., Babalola, C. O., Femi-Oyewo, M. N. & Balogun, G. Y. Antimicrobial activity and stability of *Andrographis paniculata* cream containing Shea butter. *Nig J. Pharm. Res.* **15** (1), 9–18 (2019).
29. Limsiriwong, M., Sahamethapat, A. & Kanjanapruk, P. Development and validation of UPLC method for analysis of Andrographolide from *Andrographis paniculata* (Burm. f.) Nees. *J. Thai Trad Alt Med.* **17** (2), 153–167 (2019).
30. Cava, M. P., Chan, W. R., Stein, R. P. & Willis, C. R. Andrographolide: Further transformations and stereochemical evidence; the structure of Isoandrographolide. *Tetrahedron* **21**, 2617–2632 (1965).
31. Pramanick, S. et al. Andropanolide and isoandrographolide, minor diterpenoids from *Andrographis paniculata*: Structure and X-ray crystallographic analysis. *J. Nat. Prod.* **69** (3), 403–405 (2006).
32. Chao, W. W. & Lin, B. F. Isolation and identification of bioactive compounds in *Andrographis paniculata* (Chuanxinlian). *Chin. Med.* **5**, 17–32 (2010).
33. Xu, Y., Wei, H., Wang, J., Wang, W. & Gao, J. Synthesis of Andrographolide analogues and their neuroprotection and neurite outgrowth-promoting activities. *Bioorg. Med. Chem.* **27** (11), 2209–2219 (2019).
34. Kumar, G., Singh, D., Tali, J. A., Dheer, D. & Shankar, R. Andrographolide: Chemical modification and its effect on biological activities. *Bioorg. Chem.* **95**, 103511 (2020).
35. Liu, L., Yan, Y., Zheng, L., Jia, H. & Han, G. Synthesis and structure anti-inflammatory activity relationships studies of Andrographolide derivatives. *Nat. Prod. Res.* **34** (6), 782–789 (2020).
36. Fujita, T. et al. On the diterpenes of *Andrographis paniculata*: X-ray crystallographic analysis of Andrographolide and structure determination of new minor diterpenoids. *Chem. Pharm. Bull.* **32** (6), 2117–2125 (1984).
37. Rahman, M., Ayoob, I., Rehman, S., Bhat, K. A. & Ara, T. Microwave-assisted synthesis of Andrographolide analogues as potent β-glycosidase inhibitors. *SynOpen* **2** (2), 200–206 (2018).
38. Wen, Q., Jin, X., Lu, Y. & Chen, D. F. Anticomplement *ent*-labdane diterpenoids from the aerial parts of *Andrographis paniculata*. *Fitoterapia* **142**, 104528 (2020).
39. Wang, G. Y. et al. Two new diterpenoid lactones isolated from *Andrographis paniculata*. *Chin. J. Nat. Med.* **15** (6), 458–462 (2017).
40. Yu, B., Zhang, Z., Liu, W., Tang, T. & Wang, P. Study on stability in vitro of Andrographolide. *Chin. Tradit Med.* **24**, 331–333 (2002).
41. Lee, S. Y., Abdullah, L. C., Rahman, R. A., Abas, F. & Ching, G. H. Stability and toxicity profile of solution enhanced dispersion by supercritical fluids (SEDS) formulated *Andrographis paniculata* extract. *Braz J. Chem. Eng.* **36** (2), 969–978 (2019).
42. Masuda, T. et al. Cell differentiation-inducing diterpenes from *Andrographis paniculata* Nees. *Chem. Pharm. Bull.* **42** (6), 1216–1225 (1994).
43. Geoffrey, B. A. S., Prasana, J. C., Muthu, S., Abraham, C. S. & David, H. A. Spectroscopic and quantum/classical mechanics based computational studies to compare the ability of Andrographolide and its derivative to inhibit nitric oxide synthase. *Spectrochim Acta A: Mol. Biomol. Spectrosc.* **218** (July), 374–387 (2019).
44. Guan, H. P., Kong, L. R., Cheng, C., Lim, J. C. W. & Wong, W. S. F. Protective role of 14-deoxy-11,12-didehydroandrographolide, a noncytotoxic analogue of andrographolide, in allergic airway inflammation. *J. Nat. Prod.* **74** (6), 1484–1490 (2011).
45. Nanduri, S. et al. Synthesis and structure-activity relationships of Andrographolide analogues as novel cytotoxic agents. *Bioorg. Med. Chem. Lett.* **14** (18), 4711–4717 (2004).
46. Aromdee, C., Suebsasana, S., Ekalaksananan, T., Pientong, C. & Thongchai, S. Stage of action of naturally occurring Andrographolides and their semisynthetic analogues against herpes simplex virus type 1 in vitro. *Planta Med.* **77** (9), 915–921 (2021).
47. Aromdee, C. Modifications of Andrographolide to increase some biological activities: A patent review (2006–2011). *Expert Opin. Ther. Pat.* **22** (2), 169–180 (2012).

Acknowledgements

The research leading to these results has received funding from the National Science, Research and Innovation Fund (NSRF) (Grant No. 662A17029). The authors also want to grant support from The Thailand Science Research and Innovation Fund (DBG6280007), the Permanent Secretary of the Ministry of Higher Education, Science, Research, and Innovation (F01-683R-17-046), and further supported by the National Research Council of Thailand (N34E660176).

Author contributions

The authors W.J. and R.C. were involved in conceptualization, supervision, resources, methodology, investiga-

tion, data curation, writing- original draft preparation, reviewing and editing, and funding acquisition. N.R. and K.M were involved in the anti-inflammatory activity testing and editing. G.A.C. was involved in drafting of the manuscript and interpretating the data. S.D.S., L.N, S.C., P.H. and P.P participated in reviewing and editing.

Declarations

Competing interests

The authors declare no competing interests.

Additional information

Supplementary Information The online version contains supplementary material available at https://doi.org/10.1038/s41598-025-13652-6.

Correspondence and requests for materials should be addressed to R.C.

Reprints and permissions information is available at www.nature.com/reprints.

Publisher's note Springer Nature remains neutral with regard to jurisdictional claims in published maps and institutional affiliations.